JCI insight

RESEARCH ARTICLE

Mucosal-associated invariant and γδ T cell subsets respond to initial *Mycobacterium tuberculosis* infection

Charles Kyriakos Vorkas,[1,2] Matthew F. Wipperman,[2,3] Kelin Li,[4] James Bean,[2] Shakti K. Bhattarai,[5] Matthew Adamow,[6] Phillip Wong,[6] Jeffrey Aubé,[4] Marc Antoine Jean Juste,[7] Vanni Bucci,[5] Daniel W. Fitzgerald,[1,7,8] and Michael S. Glickman[2,9]

[1]Division of Infectious Diseases, Weill Cornell Medicine (WCM), New York, New York, USA. [2]Immunology Program, Sloan Kettering Institute, Memorial Sloan Kettering Cancer Center (MSKCC), New York, New York, USA. [3]Clinical and Translational Science Center, WCM, New York, New York, USA. [4]Division of Chemical Biology and Medicinal Chemistry, UNC Eshelman School of Pharmacy, University of North Carolina at Chapel Hill, Chapel Hill, North Carolina, USA. [5]Department of Bioengineering, University of Massachusetts, Dartmouth, North Dartmouth, Massachusetts, USA. [6]Immune Monitoring Core Facility, Ludwig Center for Cancer Immunotherapy, Sloan Kettering Institute, MSKCC, New York, New York, USA. [7]GHESKIO Centers, Port-au-Prince, Haiti. [8]Center for Global Health, WCM, New York, New York, USA. [9]Division of Infectious Diseases, MSKCC, New York, New York, USA.

Innate immune responses that control early *Mtb* infection are poorly understood, but understanding these responses may inform vaccination and immunotherapy strategies. Innate T cells that respond to conserved bacterial ligands such as mucosal-associated invariant T (MAIT) and γδ T cells are prime candidates to mediate these early innate responses but have not been examined in subjects who have been recently exposed to *Mtb*. We recruited a cohort living in the same household with an active tuberculosis (TB) case and examined the abundance and functional phenotypes of 3 innate T cell populations reactive to *M. tuberculosis*: γδ T, invariant NK T (iNKT), and MAIT cells. Both MAIT and γδ T cells from subjects with *Mtb* exposure display ex vivo phenotypes consistent with recent activation. However, both MAIT and γδ T cell subsets have distinct response profiles, with CD4$^+$ MAIT and γδ T cells accumulating after infection. Examination of exposed but uninfected contacts demonstrates that resistance to initial infection is accompanied by robust MAIT cell CD25 expression and granzyme B production coupled with a depressed CD69 and IFNγ response. Finally, we demonstrate that MAIT cell abundance and function correlate with the abundance of specific gut microbes, suggesting that responses to initial infection may be modulated by the intestinal microbiome.

Introduction

Tuberculosis (TB) remains a leading cause of global mortality from an infection (1). Understanding the innate immune mechanisms of clearance of primary *Mycobacterium tuberculosis* (*Mtb*) infection and control of latent infection are critical to definitive control over the epidemic (2) and may inform TB vaccine design and immunotherapy (3, 4). Host immune responses during *Mtb* infection involve a complex and incompletely understood immunoregulatory network that includes both innate and adaptive arms of the immune system (5, 6). CD4$^+$ T cells were identified as a key component of the immune response that contains *Mtb* during latency (7, 8), although the exact effector mechanisms by which CD4$^+$ T cells prevent reactivation are still being elucidated (9, 10). CD8$^+$ T cells represent up to 40% of cells in *Mtb* human lung granulomas and may also play a role in control of infection through TCR selection, clonal expansion, and cell-mediated cytolysis (11, 12).

Our investigation focuses on the role of innate-like T cells that express conserved T cell receptors (TCR) and respond to microbially derived, nonpeptide antigens, as they may be recruited early during the host response to *Mtb* and contribute to clearance (13, 14). Of the subsets that highly express the C-type lectin receptor CD161 and respond to *Mtb*, the most intensely studied in mice are the invariant NK T (iNKT) cells, which are present at low abundance in humans (<1% T cells) and are activated by mycobacterial lipids from the *Mtb*

Conflict of interest: MG and VB have received consulting fees from Vedanta biosciences.

License: Copyright 2018, American Society for Clinical Investigation.

Submitted: April 30, 2018
Accepted: August 29, 2018
Published: October 4, 2018

Reference information:
JCI Insight. 2018;3(19):e121899. https://doi.org/10.1172/jci.insight.121899.

cell wall through a conserved TCR restricted by CD1d (15). iNKT cells have been shown to inhibit intracellular growth of *Mtb* through granulocyte-macrophage–CSF (GM-CSF) production (16). In a macaque model, $CD8^+$ iNKT cell abundance directly correlated with a resistance phenotype to *Mtb* challenge (17). Whereas iNKT cells have been shown to be depleted from the blood in active pulmonary TB (18–20), their role during early responses to initial human *Mtb* infection is not well understood.

The most abundant of $CD161^{++}$ innate-like T cells are mucosal-associated invariant T (MAIT) cells that compose 1%–18% of the peripheral T cell compartment in humans and are enriched at mucosal sites such as gut, lung, and liver (21–23). They are evolutionarily conserved in mammals and express a conserved TCR (TRAV1–2 in humans) (22) with oligoclonal Vβ chain usage (24–26). MAIT cells recognize vitamin B metabolite intermediates synthesized by a broad range of microbes, including *Mtb*, when presented by the MHC-1–related protein, *MR1* (27, 28). MAIT cells are also activated and enriched at disease sites in autoimmunity and cancer (29–32). Importantly, MAIT cell differentiation is thought to be dependent upon the microbiota, as no mature MAIT cells are detected in germ-free mice (22). However, the presence of MR1-reactive $TRAV1\text{-}2^+CD161^{++}$ cells in fetal tissue also suggests microbiota-independent mechanisms for MAIT cell selection using endogenous MR1 ligands (33). After stimulation with MR1-presented ligand, MAIT cells are rapidly activated (21, 23, 34, 35) and can secrete IFNγ, TNFα, and IL-17 and release granzyme B/perforin (21, 35, 36); however, their specific roles during *Mtb* infection is not well understood (37–40).

In patients with active pulmonary TB, MAIT cells are numerically depleted in peripheral blood compared with healthy donors (38, 39) and 1 study also reported low abundance of MAIT cells in TB pleural fluid compared with that found in the peripheral blood of healthy donors (37). MAIT cell number has been found to be inversely correlated with markers of TB disease activity, such as high levels of sputum positivity and systemic markers of inflammation (39). Additionally, peripheral blood MAIT cells were found to be functionally deficient in production of cytotoxic molecules and cytokines such as IFNγ in patients with active pulmonary TB (38). PD-1 MAIT cell expression has been associated with active TB and declines with TB treatment (37). More recently, MR1 locus variants located within the enhancer region regulating expression have been associated with susceptibility to TB meningitis and mortality (41).

These data suggest that MAIT cells are involved in the immune response during active TB and that they are either depleted after *Mtb* infection or that decreased MAIT cell abundance may precede *Mtb* reactivation. The ability of MAIT cells to recognize a conserved ligand of bacterial metabolism and their association with mucosal sites of infection supports the idea that they may be part of the innate cellular response to early infection. However, there is little human evidence examining this hypothesized role during the innate immune response to initial *Mtb* infection, as most studies were performed in cases of reactivation TB (37–39). Recently, both MAIT and iNKT cells were found to be more abundant in latent TB cases compared with uninfected controls (42). Another study reported decreased $IL\text{-}17^+CD8^+$ MAIT cells in persistently IFNγ release assay–negative ($IGRA^-$) healthy household contacts compared with IGRA converters, suggesting that $CD8^+$ MAIT cells may be protective against initial infection (40).

Another well-described innate T cell subset that responds to *Mtb* are Vγ9Vδ2 T cells that recognize microbially derived phosphoantigens and are abundant in humans, composing the majority of γδ T cells (43). Vγ9Vδ2 T cells are activated rapidly after phosphoantigen stimulation, express TNFα and IFNγ, and become enriched within the γδ T cell subset (44). These cells are postulated to exert a regulatory role during *Mtb* infection through production of IFNγ and IL-10 (45). It has also been shown that adoptive transfer of Vγ9Vδ2 T cells activated by bacillus Calmette-Guérin (BCG) immunization/phosphoantigen/IL-2 protects against *Mtb* infection in a macaque model (43, 46). However, their role in early human infection is not well understood.

Herein, we designed a cohort of healthy household contacts of active pulmonary TB patients in Port-au-Prince, Haiti, to interrogate innate T cell responses during early *Mtb* exposure. We developed ex vivo assays using peripheral blood mononuclear cells (PBMCs) to assess differences in γδ T, iNKT, and MAIT cell phenotypes of newly infected and uninfected contacts compared with unexposed community donors, also with and without latent TB infection (LTBI). We also correlated immunologic profiles with stool microbiome–derived 16S rDNA profiles to investigate microbial correlates of innate-like T cell immunity. We demonstrate that both MAIT cells and γδ T cells respond to early *Mtb* exposure, but with distinct activation profiles within the $CD4^+$ and $CD8^+$ subsets. We demonstrate distinct MAIT cell phenotypes between subjects with early latency compared with those exposed to *Mtb* but who remain uninfected. Finally, we

Table 1. Sociodemographic variables of healthy household TB contact and community control study populations

	Controls $n = 45$	TB contacts $n = 31$	*P* value
Female (%)	32 (71)	23 (74)	NS
Age, mean (range)	31 (18–52)	37 (11–62)	NS
IGRA$^+$ (%)	28 (62)	19 (61)	NS
Median number of persons in household (range)	5 (1–11)	6 (1–10)	NS
No household income	22 (49)	18 (58)	NS
Median range household income/month (USD)	77–384	77–384	NS
Median income of household/month (USD; range)	153 (38–767)	123 (61–230)	NS
No personal income (%)	5 (11)	2 (6)	NS
Ever smoker (%)	2 (4)	1 (3)	NS
Weekly alcohol consumption (%)	4 (9)	2 (6)	NS
Median AFB smear of household active TB case	NA	2–3+	–
Sleep in same house with active TB case	NA	31 (100)	–
Sleep in same room with active TB case	NA	18 (58)	–
Sleep in same bed with active TB case	NA	2 (6)	–

USD, US dollars; AFB, acid fast bacilli. Continuous variables were compared using 2-tailed unpaired *t* tests, and categorical variables were compared by χ^2 test ($P < 0.05$).

also show that innate-like T cell abundance and reactivity is correlated with gut microbiome composition, suggesting that MAIT cell responses to *Mtb* infection may be modulated by the intestinal microbiome.

Results

A cohort of recently exposed household contacts of active pulmonary TB cases to examine innate T cell responses during early infection. To study the earliest phase of TB infection, we designed a cross-sectional study of a clinical cohort of healthy household contacts of active pulmonary TB patients. The majority of contacts were recruited close to the time of diagnosis of the index case and were living in the same house as the active TB case for at least 1 month in the 6 months prior to diagnosis (median time to contact recruitment from TB case diagnosis, 2.4 months; range, 0.2–26 months). Healthy donors without reported TB exposure from the same community were recruited as controls. Of the 92 household contacts and 591 community controls enrolled to date, we randomly sampled an age-, sex-, and IGRA-matched subset of 31 TB household contacts and 45 unexposed community controls recruited between 2015 and 2017 based on PBMC, stool specimen availability, and quality control. All available specimens from IGRA$^-$ contacts (12 of 31; 39%) were assessed.

The median smear grade of the active pulmonary TB cases in the households was 2–3+. Age, sex, IGRA status, and relevant sociodemographic variables are summarized in Table 1. There were no differences in number of household members, household income, smoking status, or alcohol consumption between groups. Eighteen of 31 (58%) contacts also slept in the same room as the active pulmonary TB index case, of which 8 of 18 (44%) remained IGRA$^-$. Overall, we found more IGRA$^+$ subjects in the overall household contact cohort compared with community controls (65 of 92 [81%] vs. 443 of 591 [52%]; $P < 0.001$), consistent with 1 previous household contact study that compared latent infection prevalence with the unexposed, endemic population (47). This enhanced rate of IGRA-positivity in our contact cohort suggests enrichment for recently infected individuals and may indicate that IGRA$^-$ contacts may be exposed, but uninfected. Among the twelve IGRA$^-$ contacts enrolled, no IGRA$^+$ conversion was detected during 6-month follow-up IGRA testing.

γδ T cell subsets differentially respond to early Mycobacterium TB infection. We evaluated abundance and activation phenotypes in γδ T cells using the gating strategy in Figure 1A. The numerically dominant γδ T cell population expresses no coreceptor, but CD4$^+$ and CD8$^+$ γδ T cells are detectable in healthy donors (48). We enumerated each γδ subset as a fraction of the T cell compartment with the same coreceptor (e.g., CD8$^+$TCRγδ$^+$/CD8$^+$CD3$^+$ cells) and found no difference between contacts and controls in the abundance of total TCRγδ$^+$, CD8$^+$, or double-negative (DN) γδ cells (Supplemental Figure 1, A–C; supplemental material available online with this article; https://doi.org/10.1172/jci.insight.121899DS1). However, we observed an accumulation of CD4$^+$ γδ T cells in contacts, a difference that was present only in the IGRA$^+$ contacts

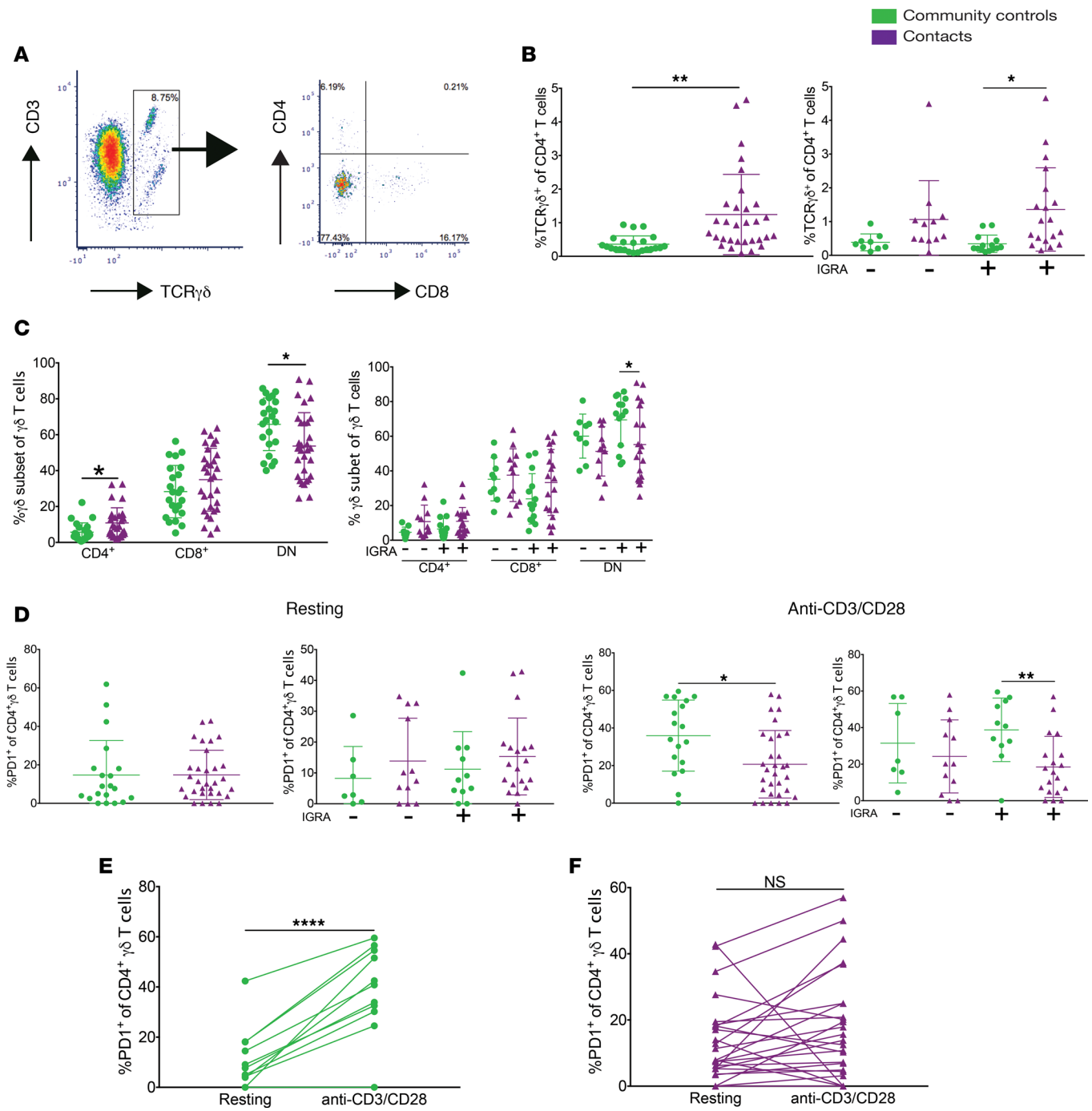

Figure 1. γδ T cells respond early to *Mycobacterium tuberculosis* infection. (**A**) Density plots demonstrating the gating strategy for γδ T cells in 1 healthy Haitian donor: left panel is gated on live cells, and right panel is gated on live CD3⁺TCRγδ⁺ cells. (**B**) TCRγδ staining in CD4⁺ T cells (left) with IGRA stratification (right) in community controls (green) and household contacts (purple). Color coding applies to all panels. Data in **B–F** represent mean ± SD. (**C**) Relative abundance of TCRγ subsets within their respective T cell subsets (left) with IGRA stratification (right). (**D**) PD-1 staining in CD4⁺ γδ T cells after 15 hours of rest (left) or anti-CD3/CD28 stimulation (right). Groups were compared by 2-tailed unpaired *t* test in **A–D** with significance level of $P < 0.05$. CD4⁺ γδ T cell PD-1 staining before or after anti-CD3/CD28 activation in IGRA⁺ community controls (**E**) and contacts (**F**). Groups were compared by 2-tailed paired *t* test in **E** and **F** with significance level of $P < 0.05$. *$P < 0.05$, **$P < 0.005$, ****$P < 0.0001$. IGRA, IFNγ release assay

(Figure 1B), indicating that this finding is specific for recently acquired latent infection. Within the γδ compartment, we found relative accumulation of CD4⁺ γδ T cells in contacts, whereas DN γδ T cells were relatively depleted, the latter being limited to the IGRA⁺ contacts (Figure 1C).

We next examined the activation status and potential of γδ T cells. CD4⁺ γδ T cells from controls strongly upregulated PD-1 with activation (Figure 1, D–F). In contrast, CD4⁺ γδ cells from contacts

expressed varying levels of PD-1 at baseline but did not substantially upregulate PD-1 upon activation (Figure 1, D–F). CD8$^+$ and DN γδ T cells also demonstrated impaired upregulation of PD-1, in addition to CD69 after ex vivo activation (Supplemental Figure 1, D–G). This blunted activation in γδ T cell subsets was limited to IGRA$^+$ contacts. Taken together, these results indicate that early LTBI activates γδ T cell subpopulations to different extents with enhanced numbers of CD4$^+$ γδ cells, which are poorly activated ex vivo. DN γδ T cell abundance appears to be reciprocally controlled by early *Mtb* infection, with depletion of the DN subset, which — along with CD8$^+$ γδ T cells — are also poorly activated ex vivo. We did not detect any γδ T cell responses in IGRA$^-$ contacts that differed from community controls.

Lack of an iNKT cell response to early Mtb infection. We next interrogated iNKT cell subset abundance and activation phenotypes as above, using the gating strategy in Supplemental Figure 2A. iNKT cell abundances were low in all donors (Supplemental Figure 2, B–D). No differences in abundance or activation of iNKT subsets were detected when comparing contacts with controls at baseline or after in vitro stimulation (Supplemental Figure 2, E and F).

Differential activation potentials of MAIT cell subsets. To profile the abundance and activation status of MAIT cells in household contacts and controls, we used 5-OP-RU–loaded MR1 tetramers to identify MAIT cells and deployed an ex vivo activation assay with MR1 ligand, 5-A-RU/MeG (35, 49). MAIT cells were identified as tetramer$^+$CD161^{++} (Figure 2A). Control staining experiments with MR1-6FP tetramers, which do not bind the MAIT cell TCR (50), demonstrate that MR1-5-OP-RU tetramers specifically identify MAIT cells (Supplemental Figure 3). Flow cytometric gating strategies for MAIT cells and their activation/effector markers are summarized in Supplemental Figure 4. Analysis of coreceptor expression in healthy donors revealed the majority of MAIT cells to be CD8$^+$, with minor subsets of DN and CD4$^+$ MAIT cells also observed, consistent with prior reports (33, 51, 52) (Figure 2, A and B). Activation did not change the subset distribution, either within the MAIT cell compartment or within the CD3$^+$ T cell compartment in healthy donors (Figure 2, C and D). Activation of MAIT cells is accompanied by TCR downregulation and CD69 upregulation, a response that is blocked by neutralizing antibodies to MR1, confirming that the activation is due to the ligand presented on MR1 (Figure 2E). However, MAIT cell subsets are not activated equivalently by ligand. We observed that CD8$^+$ and DN MAIT cells are activated by 5-A-RU/MeG in an MR1-dependent manner, as measured by either CD69 (Figure 2E) or CD25 (Figure 2F), but that CD4$^+$ MAIT cells do not upregulate activation markers with the same stimulus. We also observed that a subset of CD4$^+$ MAIT cells express the IL-2Rα chain, CD25, at baseline, whereas CD8/DN MAIT are CD25$^-$ at rest (Figure 2F). Activated MAIT cell subsets also upregulate PD-1, granzyme B, and IFNγ to varying degrees (Figure 2, G–I). These data indicate heterogeneity of MAIT cell subset resting phenotypes, as well as responses to antigen-specific stimulation.

We next examined MAIT cell phenotypes in household contacts recently exposed to an active TB patient. There was no difference in the abundance of MAIT cells in contacts compared with controls, although the average MAIT cell abundance was 1% of total T cells (range 0.1%–3.3% of T cells), somewhat lower than reported MAIT cell abundance in non-Haitian populations (Figure 3A) (37–39). When activated with ligand, however, CD8$^+$ MAIT cell TCR downregulation was enhanced, consistent with a primed state from prior activation, a finding that was only present in IGRA$^+$ contacts (Figure 3B). These results suggest that CD8$^+$ MAIT cells from IGRA$^+$ contacts are more reactive to antigen restimulation (53). In contrast, CD4$^+$ MAIT cells were relatively enriched among tetramer$^+$CD161^{++} cells of IGRA$^+$ contacts, both at rest and after antigen stimulation, either in comparison with IGRA$^+$ control subjects or IGRA$^-$ household contacts (Figure 3C). DN MAIT cells were also relatively enriched at rest; however, this finding did not correlate with IGRA status (Supplemental Figure 5, A–C).

Examination of the activation markers CD69 and CD25 on MAIT cells and their subsets revealed that upregulation of CD69 after 5-A-RU/MeG stimulation was suppressed in contacts compared with community controls (Figure 3D). Surprisingly, MAIT cells of IGRA$^-$ contacts displayed a blunted early activation response when compared with IGRA$^-$ community controls (Figure 3D), and this finding was attributable to the CD8$^+$ MAIT cell subset (Figure 3E). At baseline, we detected a prominent enrichment of CD4$^+$, but not CD8$^+$, MAIT cells expressing CD25 in contacts (Figure 3F). When analyzed by IGRA status, this CD25$^+$CD4$^+$ MAIT population was significantly enriched in IGRA$^+$ contacts in comparison with IGRA$^+$ controls (Figure 3F). With ligand activation, CD4$^+$ MAIT cells of IGRA$^+$ contacts consistently expressed more CD25 than IGRA$^+$ controls (Figure 3F), although there was no significant upregulation of CD25 among CD4$^+$ MAIT cells after 5-A-RU/MeG in a paired analysis (Figure 3, G and H). Although we could

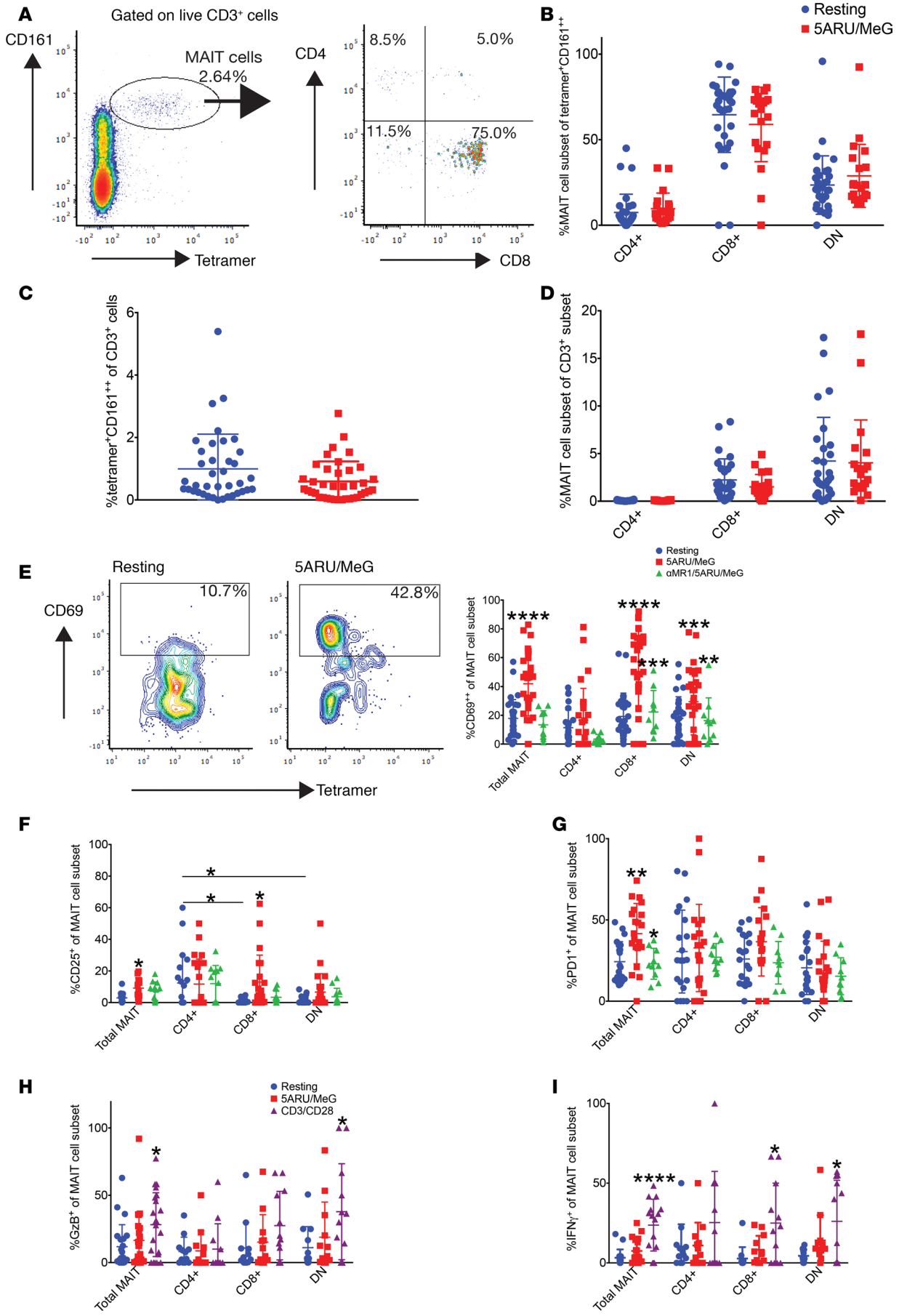
A
Gated on live CD3+ cells
CD161
MAIT cells
2.64%
Tetramer
CD4
8.5%
5.0%
11.5%
75.0%
CD8
B
Resting
5ARU/MeG
%MAIT cell subset of tetramer+CD161++
CD4+
CD8+
DN
C
%tetramer+CD161++ of CD3+ cells
D
%MAIT cell subset of CD3+ subset
E
Resting
5ARU/MeG
CD69
10.7%
42.8%
Tetramer
αMR1/5ARU/MeG
%CD69++ of MAIT cell subset
Total MAIT
F
%CD25+ of MAIT cell subset
G
%PD1+ of MAIT cell subset
H
CD3/CD28
%GzB+ of MAIT cell subset
I
%IFNγ+ of MAIT cell subset

Figure 2. MAIT cell subsets demonstrate functional heterogeneity in healthy Haitian donors. (**A**) Density plots demonstrating the gating strategy for MAIT cells in 1 healthy Haitian donor: left panel is gated on live CD3$^+$ cells, and right panel is gated on live CD3$^+$MR1-5-A-RU/MeG tetramer$^+$CD161^{++}. (**B**) Relative abundance of MAIT cell subsets among tetramer$^+$CD161^{++} cells after 15 hours of rest (blue) or 5-A-RU/MeG activation (red) in 32 healthy Haitian donors. Same donors assessed in **B–I**. Same color coding applies to **C** and **D**. Data in **B–D** and **F–I** represent mean ± SD. (**C**) Abundance of MAIT cells among T cells. (**D**) Abundance of MAIT cells within their respective T cell subset. (**E**) Contour plots demonstrating the gating strategy for MAIT cell CD69 staining, a T cell activation marker, at rest or after 5-A-RU/MeG (left panels). Both plots are gated on live, CD3$^+$, tetramer$^+$CD161^{++}. The right panel demonstrates CD69 staining in MAIT cell subsets at rest (blue), after 5-A-RU/MeG activation (red), or after treatment with neutralizing αMR1 antibody for 1 hour prior to 5-A-RU/MeG activation (green). Same color coding applies to **F** and **G**. (**F**) CD25 and (**G**) PD-1 staining in MAIT cell subsets. (**H**) GzB and (**I**) IFNγ measured by intracellular staining in the resting (blue), 5-A-RU/MeG (red), and anti-CD3/CD28 (purple) conditions in MAIT cell subsets. Groups were compared by 2-tailed unpaired *t* test with a significance level of $P < 0.05$. Asterisks above stimulated conditions indicate statistical significance compared with resting. Asterisks above the αMR1 condition indicate statistical significance compared with the 5-A-RU/MeG-stimulated condition. *$P < 0.05$, **$P < 0.005$, ***$P < 0.0005$, ****$P < 0.0001$; 5-A-RU, 5-amino-6-(D-ribitylamino)uracil; MeG, methylglyoxal; GzB, granzyme B.

not detect differences in the mean abundance of CD25$^+$CD8$^+$ MAIT cells between groups at baseline or after 5-A-RU/MeG activation (Figure 3F), paired analysis revealed that CD8$^+$ MAIT cells of IGRA$^-$ contacts, but not IGRA$^+$ contacts, significantly upregulated CD25 after MR1-ligand stimulation compared with IGRA-matched controls (Figure 3, G and H). Taken together, these results suggest that CD4$^+$ MAIT cells constitutively express CD25 during early latent infection, whereas CD8$^+$ MAIT cell expression of CD25 is a marker of exposed but uninfected contacts. No differences in activation were detected in DN MAIT cells (Supplemental Figure 5, D–F).

We next examined effector function of MAIT cells in contacts. Although there was no difference in the mean proportion of granzyme B$^+$ MAIT cells between groups with 5-A-RU/MeG or anti-CD3/CD28 stimulation, paired analyses revealed that MAIT cells from IGRA$^+$ contacts demonstrated impaired granzyme B production (Figure 4A) and robust IFNγ production (Figure 4B). In contrast, MAIT cells of IGRA$^-$ contacts, who had resisted infection, displayed strong granzyme B production (Figure 4A) and suppressed IFNγ responses (Figure 4B). To control for T cell anergy or inefficiencies of our activation assay, we also analyzed IFNγ responses of CD8$^+$ T cells with mitogen and observed the expected upregulation of this cytokine after anti-CD3/CD28 in all clinical subgroups (Figure 4C), demonstrating that the differences in effector function observed above are specific to the MAIT cell compartment.

Taken together, these data indicate that MAIT cells respond early to *Mtb* infection and that subsets defined by their TCR coreceptor adopt distinct phenotypes during the innate response to early *Mtb* infection. CD8$^+$ MAIT cells show evidence of prior activation and are relatively depleted among contacts with early latent infection, whereas CD4$^+$ MAIT cells are relatively abundant, suggesting that they respond differentially to *Mtb* exposure. Further, CD25$^+$CD4$^+$ MAIT cells accumulate in IGRA$^+$ contacts, whereas CD8$^+$ MAIT cells upregulate CD25 after antigen-specific stimulation in IGRA$^-$ contacts. Importantly, granzyme B and IFNγ MAIT effector function distinguished between IGRA$^+$ and IGRA$^-$ contacts, with robust Granzyme B expression defining those resistant to initial infection.

Innate-like T cell subset abundance and function correlate with distinct intestinal microbiome 16S rDNA signatures. In humans, it is not fully understood what factors determine the numerical abundance and reactivity of T cells of a given subset. Multiple studies support an interdependence of gut microbiome composition and peripheral immunity (54–56); thus, we reasoned that gut microbiome composition might correlate with innate T cell abundance and that these correlations are a potential marker of relationships between specific gut microbial constituents and innate immunity. Further, we hypothesized that correlations between gut microbial composition and innate immune responses may predict individual responses to *Mtb* exposure.

To first assess differences in gut microbial composition between contacts and controls, we performed t-distributed stochastic neighbor embedding (t-SNE) ordination of 22 family contacts and 28 community control stool 16S rDNA sequencing data using Jensen–Shannon divergence. We found that 16S rDNA signatures of contacts separated well from controls (Figure 5A), suggesting compositional differences in the gut microbiome between cohorts (Adonis test, $P < 0.001$). We then performed linear discriminant analysis effect size (LEfSe) (57) to compare microbiome composition at the 16S rDNA operational taxonomic unit (OTU) level. The relative abundance of the 29 OTUs that significantly differed between contacts and controls ($P < 0.01$; linear discriminant analysis [LDA] > 2.5) is shown in Figure 5B. The majority of bacterial orders that differed between groups were Bacteroidia and Clostridia. Overall, more OTUs were relatively depleted in contacts than controls (21 vs. 11 OTUs). Notably, 7 of 8 *Bacteroides spp*. with significantly different abundance between groups were relatively depleted in contacts.

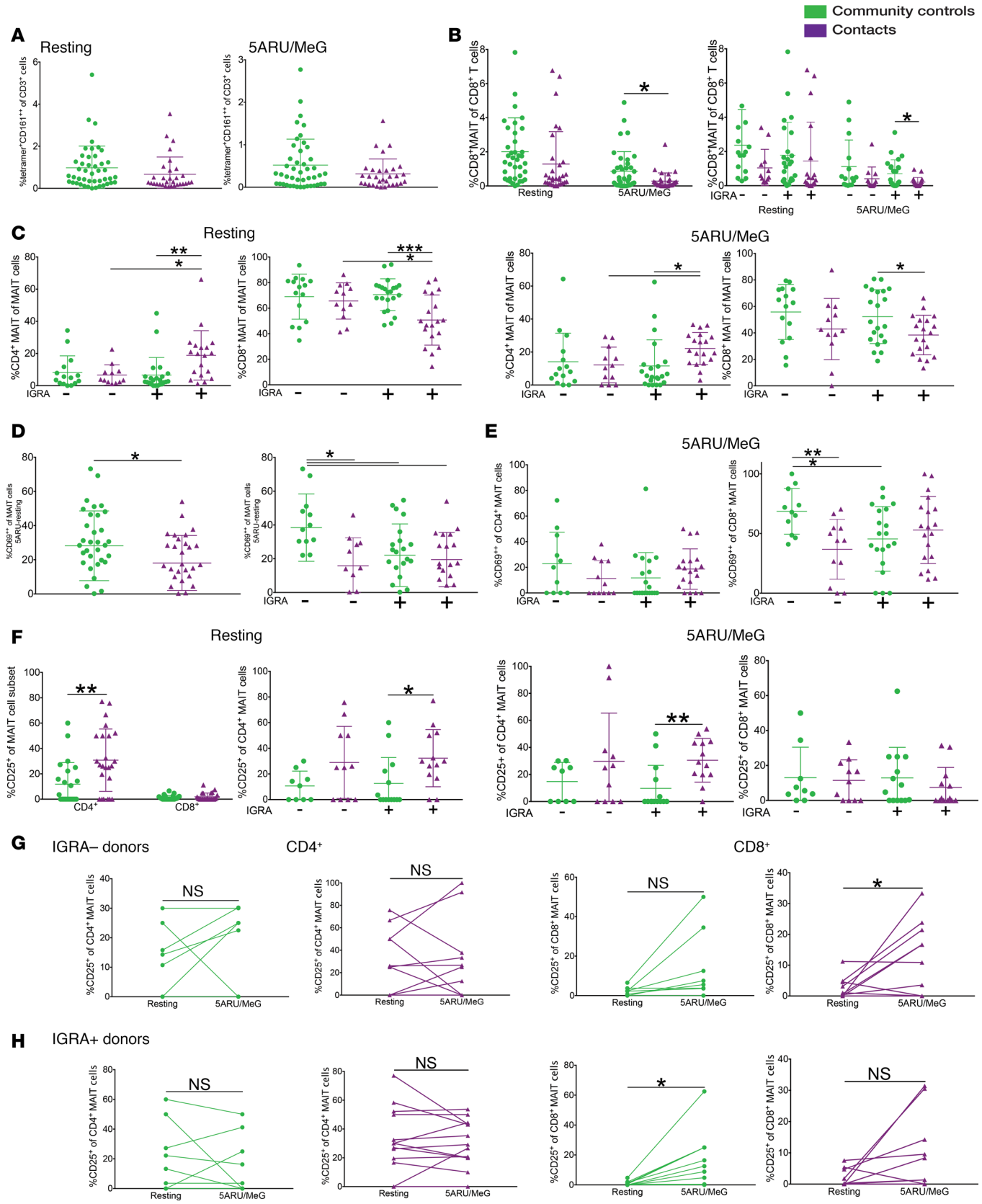

Figure 3. MAIT cell subsets respond to early *Mycobacterium tuberculosis* infection. (**A**) MAIT cell abundance among T cells after 15 hours of rest (left) or 5-A-RU/MeG activation (right) in community controls (green) and household contacts (purple). Color coding applies to all panels. Data in all panels represent mean ± SD. (**B**) CD8+ MAIT cell abundance within the CD8+ T cell subset at rest or after 5-A-RU/MeG (left) with IGRA stratification (right). (**C**) CD4+ and CD8+ MAIT cell relative abundance among MAIT cells stratified by IGRA status at rest (left) or after 5-A-RU/MeG activation (right). (**D**) Total MAIT

cell activation measured as the difference of CD69 staining in the 5-A-RU/MeG and resting conditions (left) with IGRA stratification (right). (**E**) CD69 staining in CD4$^+$ (left) and CD8$^+$ (right) MAIT cells after 5-A-RU/MeG. (**F**) Activation measured by CD25 staining in CD4$^+$ and CD8$^+$ MAIT cells with IGRA stratification at rest (left) or after 5-A-RU/MeG (right). **A–F** were analyzed by 2-tailed unpaired *t* test. (**G** and **H**) CD25 staining in CD4$^+$ MAIT (left) and CD8$^+$ MAIT (right) in IGRA$^-$ (**G**) and IGRA$^+$ (**H**) donors analyzed by 2-tailed paired *t* test. *$P < 0.05$, **$P < 0.005$, ***$P < 0.0005$. IGRA, IFNγ release assay; 5-A-RU, 5-amino-6-(D-ribitylamino)uracil; MeG, methylglyoxal.

Given the potential interdependence between the gut microbiome and peripheral immunity during *Mtb* exposure, we next asked whether bacteria that were differentially abundant between contacts and controls (Figure 5B) correlated with immune phenotypes that also differed between groups (Figure 1–4). We hypothesized that numerical abundance and activation potential of γδ T cells and MAIT cells may be correlated to specific microbial constituents. A summary of Spearman correlations ($P < 0.01$) between these overlapping microbial constituents (Figure 5B, in bold) and innate immune phenotypes are summarized in the heatmap and scatter plots presented in Figure 5C and Supplemental Figure 6, respectively. Notably, several members of the class Bacteroidia (5 *spp.*) correlated with innate immune abundance or effector function. For example, 2 Bacteroidetes, *B. ovatus* (OTUs 563 and 654) and *P. merdae* (OTU 29), were relatively depleted in contacts and strongly positively correlated with the Granzyme B inducibility of MAIT cells, an immune phenotype we have found to be depressed in recently infected contacts (Figure 4A). In contrast, the Gammaproteobacteria *S. dextrinosolvens* (OTU 19) was relatively abundant in contacts and correlated with CD4$^+$ MAIT cell abundance, a cell subset enriched in contacts. Other classes that correlated with immune phenotypes included Clostridia (OTUs 32 and 646), Erysipelotrichia (OTU 4), Negativicutes (OTU 77), and Verrucomicrobiae (OTU 11).

Discussion

The earliest phase of the *Mtb* infection cycle, inhalation of aerosolized *M. tuberculosis* from the cough of an individual with active pulmonary TB, is clinically silent and results in the establishment of latent infection in many exposed contacts. In some contacts, who remain uninfected despite exposure, it is widely speculated that innate immune mechanisms may confer resistance to infection by eliminating *Mtb* before establishment of LTBI and preventing the adaptive T cell responses that accompany it. In both cases, the earliest innate immune mechanisms that respond to *Mtb* are poorly understood, but defining these mechanisms is critical to designing vaccination strategies that could prevent initial infection and the establishment of latency. Innate-like T cells that respond to conserved microbial ligands are prime candidates to respond to early *Mtb* infection due to their high precursor frequency, specificity for conserved microbial metabolites, and diverse effector functions. Through analysis of innate-like T cell responses of TB healthy household contacts and unexposed donors from the same community, we provide evidence that γδ T cell and MAIT cell subsets respond early to *Mtb* exposure and that subsets of these innate-like T cells have distinct phenotypes during primary *Mtb* exposure and infection.

It has long been recognized that γδ T cells expand early during *Mtb* infection (58). In primates, this expansion is clonal and selects for Vγ9$^+$Vδ2$^+$ TCR usage, which is — at baseline — the most abundant γδ TCR (59). This clonal expansion occurs in response to phosphoantigens conserved among mycobacteria (60) in an MHC II–independent, butyrophilin-dependent manner (61, 62). These data indicate that Vγ9Vδ2 T cells are selected during ontogeny and are poised to respond quickly to primary *Mtb* exposure. Whereas both *Mtb*-derived and purified phosphoantigen induce Vγ9Vδ2 T cell proliferation, only a subset of these cells can inhibit Mtb growth (63), which is consistent with functional heterogeneity among Vγ9Vδ2 T cells, despite uniform TCR usage. Clonal immune responses of *Mtb*-specific Vγ9Vδ2$^+$ T cells in macaques have been detected by CDR3 spectratyping and demonstrate differential distribution in tissues associated with stage of infection (44). The contribution of γδ T cell coreceptor usage to *Mtb*-specific responsiveness has not been well tested, as most studies in TB did not subtype these cells with CD4 or CD8 coexpression (40, 46, 58, 63–65). Moreover, differential responses of γδ T cell subsets associated with CD4 or CD8 coexpression have not been studied in a household contact cohort (40).

Although there were no differences in total γδ T cell abundance between groups, we did observe a significant expansion of CD4$^+$ γδ T cells in recently infected contacts, consistent with 1 previous report of preferential expansion of CD4$^+$Vγ2$^+$ cells in healthy healthcare worker TB contacts compared with endemic, unexposed donors (48). Further, we observed depressed CD4$^+$ γδ T cell–functional responses

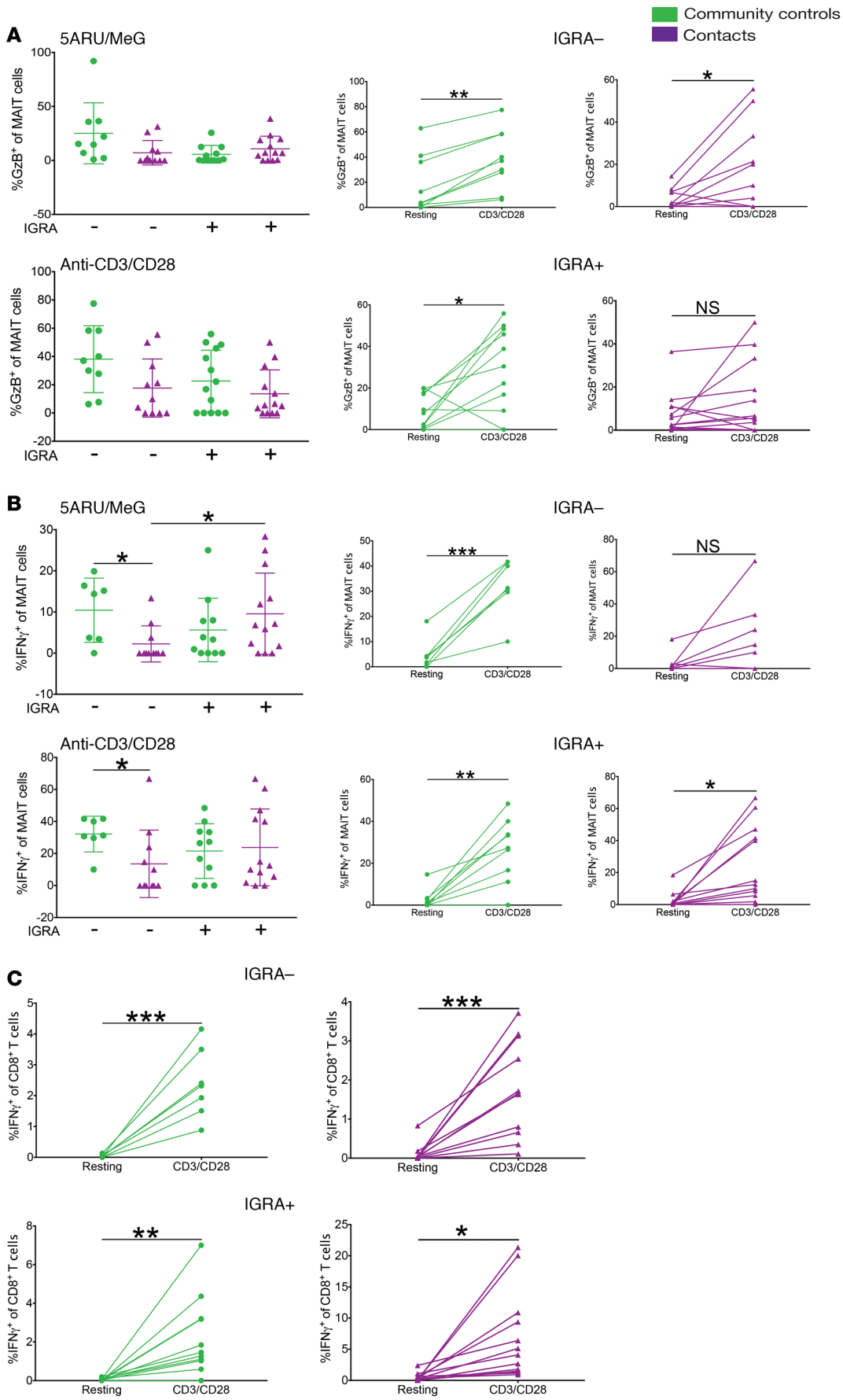

Figure 4. MAIT cell effector function distinguishes uninfected and latently infected contacts. MAIT cell GzB (**A**) and IFNγ (**B**) measured by intracellular staining in the 5-A-RU/MeG and anti-CD3/CD28 stimulation conditions stratified by IGRA status in community controls (green) and household contacts (purple). Color coding applies to all panels. Analysis was performed by 2-tailed unpaired *t* test (left) and 2-tailed paired *t* tests in the anti-CD3/CD28 condition in IGRA⁻ and IGRA⁺ donors (right). Data in all panels represent mean ± SD. (**C**) CD8⁺ T cell IFNγ measured by intracellular staining in a paired analysis of the resting and anti-CD3/CD28 conditions stratified by IGRA status. $^{*}P < 0.05$, $^{**}P < 0.005$, $^{***}P < 0.0005$. GzB, granzyme B; IGRA, IFNγ release assay.

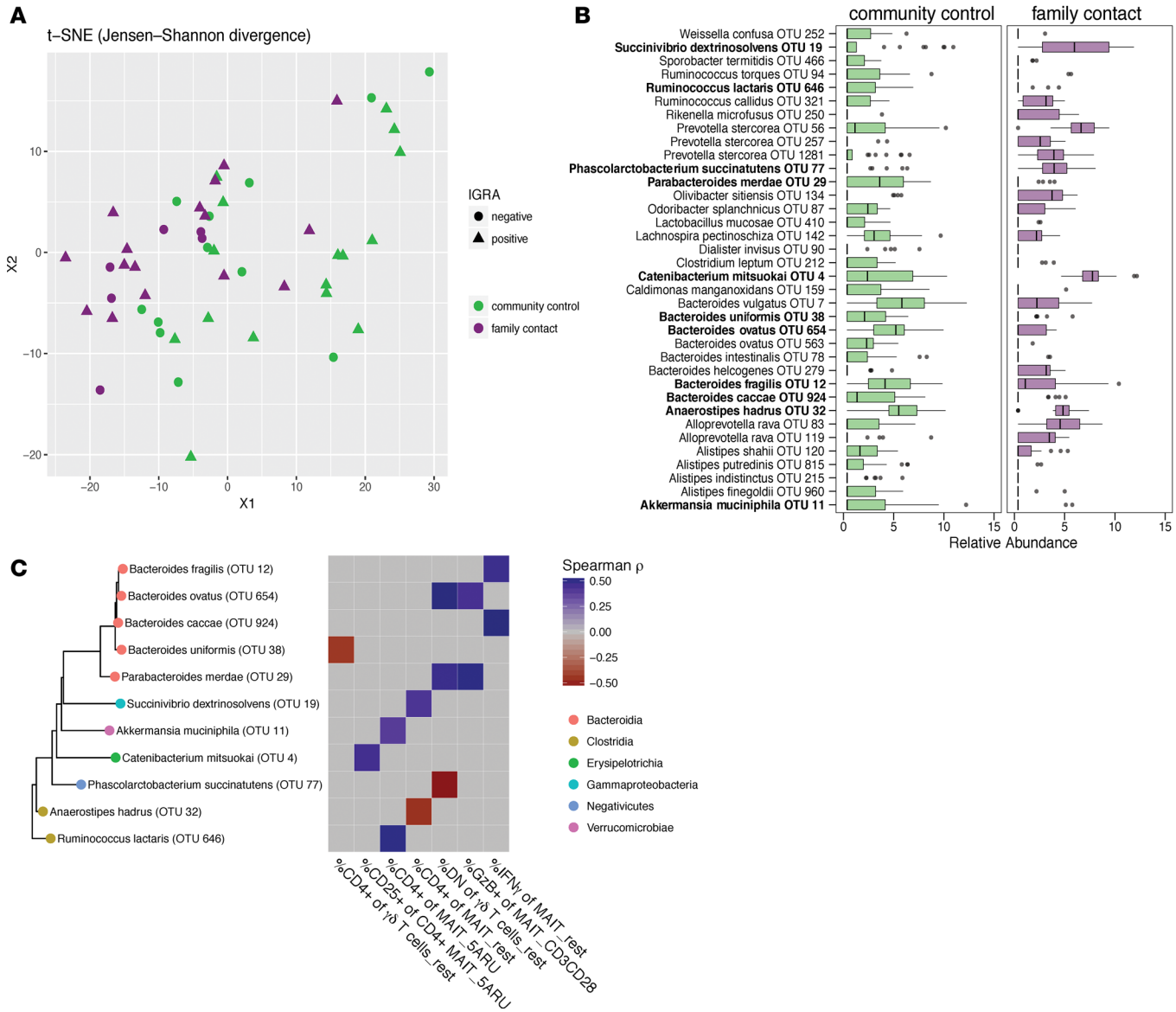

Figure 5. TB contacts and unexposed controls have distinct gut microbial signatures. (**A**) t-Distributed Stochastic Neighbor Embedding (t-SNE) ordination of 22 family contacts (purple) and 28 community controls (green), compared using 16S rDNA OTU data. IGRA$^+$ donors are represented by triangles and IGRA$^-$ donors by circles. The dissimilarity measure used was Jensen–Shannon divergence. (**B**) LEfSe was used to compare microbiome composition at the 16S OTU level. The relative abundance of significant OTUs ($P < 0.01$; LDA > 2.5) was plotted as a notched box plot. The lower and upper hinges correspond to the 25th and 75th quartiles, the whiskers extend to 1.5× the interquartile range, and dots are outliers. The line is the median relative abundance. (**C**) OTUs that were differentially abundant between community controls and family contacts ($P < 0.01$; **B**) were each independently correlated with immune phenotypes that also differed between cohorts (Figures 1–4). The phylogenetic tree, derived from 16S sequencing data, shows the organisms that met both criteria (also highlighted in bold in **B**). The tips of the tree are colored according to the class of the OTU assignment using BLAST. The heatmap shows the Spearman correlation coefficient for each OTU compared with each immune phenotype. OTU, operational taxonomic unit; IGRA, IFNγ release assay; LEfSe, linear discriminant analysis effect size; BLAST, basic local alignment search tool.

in vitro, suggesting that this subset may be exhausted from prior in vivo activation from *Mtb* exposure. We also observed that DN γδ T cells were relatively depleted in contacts, and both DN and CD8$^+$ γδ T cell subsets were also functionally depressed during in vitro stimulation. These results indicate that all 3 subsets seem to respond to *Mtb* infection, whereas only CD4$^+$ γδ T cells undergo clonal expansion. Taken together, these data suggest that CD4$^+$ γδ T cell expansion, accompanied by relative DN γδ T cell depletion, are biomarkers of early latent infection. The absence of this population in latently infected individuals without recent exposure strengthens the conclusion that the reactivity of this γδ T cell population occurs early after aerosol exposure and then recedes during later stages of latent infection.

Importantly, we did not detect evidence of prior γδ T cell activation or accumulation in IGRA$^-$ contacts, indicating that activation and expansion of this subset may not correlate with early responses to *Mtb* that prevent latent infection. This finding is consistent with 1 childhood TB study that failed to detect peripheral γδ T cell expansion to phosphoantigen in healthy purified protein derivative–negative (PPD$^-$) children compared with healthy PPD$^+$ children (66). Taken together, these results indicate that *Mtb* exposure alone is not sufficient to activate *Mtb*-specific γδ T cell subsets and that these cells respond during establishment of initial latency.

Selective expansion of the Vγ9Vδ2 subset in macaque *Mtb* infection models with BCG immunization (43), IL-2 (46), and adoptive transfer experiments (65) have been shown to be protective against *Mtb* challenge, making these cells an attractive target for TB vaccine design or immunotherapy. However, CD4 and CD8 coexpression within the Vγ9Vδ2 subset in macaques was not evaluated in these studies. Our data highlights the importance of investigating TCR coreceptor heterogeneity among *Mtb*-specific γδ T cells. While we did not assess cytokine-specific responses among γδ T cells, previous studies indicate that the Vγ9Vδ2 subset is multifunctional and can produce IFNγ, TNFα, and IL-17, as well as IL-10 (40, 45, 67). Further investigation of cytokine-specific responses within γδ T cell subsets during early *Mtb* infection is critical to understanding their functional specialization and postulated control of latent infection.

While our study did not specifically identify Vγ9Vδ2$^+$ cells among γδ T cells, the expansion and activation phenotypes observed were likely due to this subset, as it is the most common γδ TCR in humans and similar abundance/activation results were observed using pan-TCRγδ– or Vγ9Vδ2-specific gating strategies (43, 66–68). We could not exclude the presence of additional Vγ9Vδ2$^-$TCRγ$^+$ clones that may have contributed to differences in contacts.

Our study did not reveal differences in iNKT subset abundance or activation phenotype between contacts and controls in this study population, contrasting with recent findings of increased frequency of iNKT cells in latently infected individuals compared with uninfected controls (42). These data suggest that peripheral blood iNKT cells may not be a marker of early TB exposure or initial infection in these cohorts.

Several previous studies of MAIT cells and TB either did not differentiate between MAIT cell subsets (37–39) or included CD8 coexpression as a prerequisite for MAIT cell identification (40). This latter study did observe an enrichment of CD4$^+$/Vα7.2$^+$/CD161^{++} cells in LTBI subjects compared with active TB cases, but the identity of these cells was unknown. The availability of MR1-5-OP-RU tetramers (27, 35, 52) has allowed for accurate identification of MAIT cell subsets, highlighting the importance of subset heterogeneity that may not be easily detected without also staining for TCR coreceptors (51, 52). Kurioka et al. (51) assessed functional differences between CD4$^+$, CD8$^+$, and DN MAIT cells in healthy donors, demonstrating that CD8$^+$ and DN MAIT cells were more reactive and polarized toward a Th1 phenotype with *E. coli* activation, whereas CD4$^+$ MAIT cells were biased toward a Th2 phenotype, with higher levels of intracellular IL-4 and IL-13 detected by intracellular staining. The authors also report high expression of CD25 in CD4$^+$ MAIT cells, which we confirm here. Another recent study reports that CD4$^+$ MAIT cells also secrete more IL-2 than other subsets (52). Taken together, these findings highlight the importance of interrogating MAIT cells using TCR coreceptor expression as a marker of phenotypic heterogeneity.

Here, we identify previously unappreciated roles for CD4$^+$ and CD8$^+$ MAIT cell subsets during early *Mtb* exposure and infection. Increased reactivity of CD8$^+$ MAIT cells in IGRA$^+$ contacts, coupled with depressed CD69 expression and inducible CD25 expression after MR1 ligand stimulation in IGRA$^-$ contacts, supports the hypothesis that CD8$^+$ MAIT cells are primed early after *Mtb* exposure and may contribute to *Mtb* clearance. Further, mitogen-induced upregulation of granzyme B and lack of an IFNγ response in MAIT cells of IGRA$^-$ contacts suggests that clearance of primary infection could be mediated by granzyme B$^+$ MAIT cells that have been shown to detect and respond to *Mtb*-infected cells (34).

Although peripheral blood MAIT cell depletion at baseline in active pulmonary TB cases has previously been reported (37–39), we detected no significant difference in total or CD8$^+$ MAIT cell baseline abundance in TB contacts. In contrast to a recent report, we did not detect enrichment of CD8$^+$ MAIT cells in latently infected subjects (42). In contrast to the CD8$^+$ MAIT cell subset, CD4$^+$ MAIT cells were relatively enriched within the MAIT cell subset in IGRA$^+$ contacts, both at baseline and after MR1 ligand stimulation. This is consistent with previous findings that CD4$^+$ MAIT cells are less reactive to in vitro stimulation than CD8$^+$ MAIT cells (51) and, thus, become relatively enriched due to decreased abundance of CD8$^+$ MAIT cells. Consistent with previous literature in healthy donors, CD4$^+$ MAIT cells highly express the IL-2Rα chain (CD25) in the resting state relative to CD8$^+$ MAIT cells. We extend these findings to IGRA$^+$,

recently *Mtb*-exposed subjects who demonstrate increased abundance of $CD25^+CD4^+$ MAIT cells. Taken together with the inducible CD25 expression in $CD8^+$ MAIT cells of $IGRA^-$ contacts and the recent finding of increased IL-2 levels in $CD4^+$ MAIT cells (52), these data suggest a role for MAIT cell IL-2 signaling during early *Mtb* exposure and latency.

To our knowledge, MAIT cells have been investigated in only 1 household contact cohort and compared with the active TB source case from the same household rather than a healthy population from the same community. Interestingly, Coulter et al. (40) detected more intracellular IL-17 in $CD8^+$ MAIT cells of IGRA converters versus nonconverters, suggesting that IL-17–mediated inflammation is a marker of latent infection. Alternatively, inhibition of IL-17–responses may be protective against latent infection. As all of our $IGRA^-$ contacts remained $IGRA^-$ at the 6-month follow-up, we could not assess the immune phenotypes of IGRA converters. We neither found differences in IL-17/TNFα expression between $IGRA^-$ and $IGRA^+$ contacts nor when compared with unexposed controls (data not shown).

The dynamic relationship between the gut microbiota and human peripheral T cell immunity during infection is an area of active investigation (54–56) and may have important implications during immune responses to *Mtb* (69–72). It has also been observed that active TB cases on treatment have an antibiotic-induced dysbiosis of the gut microbiome that continues even after treatment is completed (70, 72), potentially explaining the increased risk for reinfection, which is noted to be of higher incidence in those who completed anti-TB therapy (73, 74).

Here, we demonstrate that microbial signatures of household TB contacts significantly differ from those of community controls. Although microbiome signatures within households may be expected to cluster, secondary to environment and diet (75, 76), we were surprised to find that household *Mtb* exposure itself is associated with differences in gut microbial composition across households. This difference could not be explained through measured socioeconomic variables such as income, smoking, or alcohol consumption as shown in Table 1. Our study design cannot determine whether these differences preceded the TB exposure or are a consequence of it, but the latter possibility would suggest that *Mtb* exposure alters gut microbial composition during the innate immune response. We further characterized the specific microbial OTU differences and show that healthy household contacts possess a relative depletion of *Bacteroides spp.* compared with community controls. This suggests that *Mtb* exposure and the immune responses that we describe herein may either induce specific changes to gut microbial composition or be a direct readout of gut microbiome composition. There is strong evidence in mice that *Bacteroides spp*. can modulate immune function (77). Specifically, polysaccharide A from *B. fragilis* has been shown to induce antiinflammatory immune responses in mouse models of disease (78). However, little is known about the mechanisms underlying how human gut microbiome components modulate innate T cell responses.

Among the innate-like T cell subsets examined, MAIT cell differentiation is thought to be most dependent on the host microbiota based on the absence of mature MAIT cells in germ-free mice (27, 79), though potential microbiota-independent MAIT cell selection in human fetal tissue has also been demonstrated (33). MAIT cells are known to respond to diverse microorganisms, including members of the healthy microbiota (23, 49, 80). There is also evidence that heterogeneity of MAIT cell responses may be associated with microbe-specific ligands, TLRs and cytokine costimulation (81–83). Additionally, iNKT and γδ T cell subset abundance and function have been associated with alterations to the microbiome (84–86).

In conclusion, our study provides important insights into innate-like T cell–mediated immunity during *Mtb* exposure and infection in a healthy household contact cohort with high prevalence of latent infection. We identify γδ T cells and MAIT cells as early responders to *Mtb* exposure and highlight the differential immune responses associated with each subset. $CD4^+$ MAIT cells and $CD4^+$ γδ T cells are enriched in recently infected subjects, suggesting that these cellular subtypes have previously unidentified roles in early innate immunity to TB. We underscore the abundance of $CD25^+CD4^+$ MAIT cells in $IGRA^+$ contacts and inducible CD25 responses of $CD8^+$ MAIT cells in $IGRA^-$ contacts, which suggest that these cellular subsets mediate early innate responses and, potentially, resistance to primary infection. In summary, our findings should encourage further longitudinal studies to determine whether the innate T cell responses identified here may correlate with the chance of later reactivation once LTBI is established. Longitudinal studies of household contacts that correlate the responses identified here with later reactivation, as well as animal models, will further test this hypothesis and potentially inform immune enhancement vaccination strategies that target innate-like T cells.

Methods

Donor recruitment and protection of human subjects. Donors were enrolled through the Tri-Institutional Tuberculosis Research Unit (TBRU) at the Groupe Haitien d'etude du Sarcome de Kaposi et des Infections Opportunistes (GHESKIO) Centers (Port-au-Prince, Haiti). A dedicated clinical field team at the GHESKIO Centers in Port-au-Prince, Haiti, recruited research volunteers as part of the NIH-funded TBRU (AI111143). LTBI was detected using QuantiFERON Gold IGRA, and active TB was excluded by clinical screening for symptoms of TB. All cases with active pulmonary TB received periodic follow-up appointments while on treatment, and anyone with known contact with an active TB patient received a 6-month follow-up and was rescreened with IGRA. All donor samples were deidentified on site using a barcode system before they were shipped to WCM/MSKCC for analysis.

Clinical characteristics of study groups from the TBRU study. We performed a cross-sectional study of healthy household contacts of active pulmonary TB patients and healthy unexposed donors from the same community. We recruited families of active pulmonary TB patients where at least 2 siblings within the family were diagnosed with active TB. These criteria were designed to select for households with high risk of transmission of *Mtb*. Household contacts were then recruited if they had been sleeping in the same house with a TB case for at least 1 month during the 6 months prior to the TB case diagnosis. Contacts underwent clinical screening for active TB symptoms and IGRA testing. Healthy donors without history of TB contacts or disease were recruited from the same community as a control group for exposure and also underwent clinical screening for active TB symptoms and IGRA testing. All donors provided informed consent prior to peripheral blood donation for PBMC isolation and stool submission for DNA extraction and 16S rDNA sequencing.

PBMC isolation. PBMCs are isolated from peripheral blood at GHESKIO (Port-au-Prince, Haiti) using the Ficoll-Paque (GE Healthcare) density centrifugation, frozen in 5×10^6 cells/ml aliquots in 90% FBS (Thermo Fisher Scientific)/10% DMSO and stored at –80°C prior to being shipped on dry ice to WCM/MSKCC.

MAIT cell ex vivo activation assay. Synthetic 5-A-RU was synthesized as previously described (35) and stored at 4°C in the solid form until dissolving in sterile, distilled H_2O and freezing at –80°C in 200 μM stock solutions. Stock solutions of 2 μM 5-A-RU•H_2O and 50 μM MeG•H_2O were prepared as needed for cell culture. Cryopreserved healthy donor PBMCs were thawed and cultured in RPMI 1640 media (ATCC)/10% FBS and directly incubated with 2 μM 5-A-RU•H_2O/50 μM MeG•H_2O for 15 hours at 37°C as previously described (35). PBMCs were stained with Zombie Red Fixable Viability Dye (BioLegend, catalog 423109) and antibodies to CD3 (UCHT1; Alexa700; eBioscience; Thermo Fisher Scientific, catalog 16-0038-81), CD161 (DX12; APC; BD Biosciences, catalog 550968), CD69 (FN50; BV421; BioLegend, catalog 310929), CD25 (BC96; BV711; BioLegend, catalog 302635), PD-1 (EH12.1; BV650; BD Biosciences, catalog 564104), CD4 (SK3; PerCPefluor or BV650; eBioscience; Thermo Fisher Scientific, catalog 46-0047-41, or BD Biosciences, catalog 563876) and CD8 (SK1; APC-H7; BD Biosciences, catalog 560179), Vγ24Jα18 (6B11; BV510; BioLegend, catalog 342917) and TCR γδ (B1; FITC; BioLegend, catalog 331207), and MR1-5-OP-RU tetramers (NIH tetramer core facility; PE or BV421) for 15 minutes at room temperature in the dark. Intracellular staining was performed using a FoxP3/Transcription Factor Staining buffer set (eBioscience, catalog 00-5523-00). Cells were permeabilized and fixed for 40 minutes at 4°C. Cells were then stained with antibodies to Granzyme B (GB11; FITC; BioLegend, catalog 515403), IFNγ (B27 or 4S.B3; PE or BV785; BioLegend, catalogs 507506 or 502541), TNFα (MaB11; BV605; BioLegend, catalog 502935), and IL-17 (BL168: BV510; BioLegend, catalog 512329) for 1 hour at 4°C. Blocking experiments were performed by incubating PBMCs directly with 5 μg/ml anti-MR1 antibody (26.5; BioLegend, catalog 361102) for 1 hour prior to incubation with 5-A-RU/MeG. Human CD3/CD28 T cell activator Dynabeads (Gibco; Thermo Fisher Scientific, catalog 111.61D) were incubated with PBMCs for 15 hours at a 1:2 bead/cell ratio. All cells were analyzed on a Fortessa Flow Cytometer (BD Biosciences).

Microbial DNA extraction from stool. DNA extraction from stool was performed as previously described (70). Stool specimens were collected and stored for less than 24 hours at 4°C, aliquoted (~2 ml each), frozen at –80°C, and shipped to WCM/MSKCC. About 500 mg of stool from frozen samples was suspended in 500 μl of extraction buffer (200 mM Tris-HCl [Thermo Fisher Scientific], pH 8.0; 200 mM NaCl [Thermo Fisher Scientific]; 20 mM EDTA [MilliporeSigma]), 210 μl of 20% SDS, 500 μl of phenol/chloroform/isoamyl alcohol (25:24:1; MilliporeSigma), and 500 μl of 0.1-mm–diameter zirconia/silica beads (Biospec Products). Samples were lysed via mechanical disruption with a bead beater (Biospec Products for 2 minutes, followed

by 2 extractions with phenol/chloroform/isoamyl alcohol [25:24:1]). DNA was precipitated with ethanol and sodium acetate at –80°C for 1 hour, resuspended in 200 µl of nuclease-free water, and further purified with QIAamp DNA Mini Kit (Qiagen) according to the manufacturer's protocols, including Protein removal by Proteinase K treatment. DNA was eluted in 200 µl of nuclease-free water and stored at –20°C.

16S rDNA sequencing. Primers used to amplify rDNA were: 563F (59-nnnnnnnn-NNNNNNNNNN-NN-AYTGGGYDTAAAGN G-39) and 926R (59-nnnnnnnn-NNNNNNNNNNNN-CCGTCAATTY-HTTTR AGT-39). Each reaction contained 50 ng of purified DNA, 0.2 mM dNTPs, 1.5 µM $MgCl_2$, 1.25 U Platinum TaqDNA polymerase, 2.5 µl of 10× PCR buffer, and 0.2 µM of each primer. A unique 12-base Golay barcode (Ns) preceded the primers for sample identification after pooling amplicons. One to 8 additional nucleotides were added before the barcode to offset the sequencing of the primers. Cycling conditions were the following: 94°C for 3 minutes, followed by 27 cycles of 94°C for 50 seconds, 51°C for 30 seconds, and 72°C for 1 minute, where the final elongation step was performed at 72°C for 5 minutes. Replicate PCRs were combined and were subsequently purified using the Qiaquick PCR Purification Kit (Qiagen) and Qiagen MinElute PCR Purification Kit. PCR products were quantified and pooled at equimolar amounts before Illumina barcodes and adaptors were ligated on using the Illumina TruSeq Sample Preparation procedure. The completed library was sequenced on an Illumina Miseq platform per the Illumina recommended protocol.

16S rDNA bioinformatics analysis. For 16S MiSeq sequencing, paired-end reads were joined, demultiplexed, filtered for quality using maximum expected error (E_{max} = 1), and dereplicated. Sequences were grouped into OTUs of 97% distance-based similarity using UPARSE (87). Potentially chimeric sequences were removed using both de novo and reference-based methods (where the Genomes OnLine Database [Gold] was used for the latter) (88). Taxonomic assignments were made using BLASTN (88) against the NCBI refseq_rna database (89). A biological observation matrix (biom) (90) file, a taxonomy file, reference sequence file, and tree file were constructed using QIIME commands. These files were imported into R (91) and merged with a metadata file into a single Phyloseq object (92). Phyloseq was used for all downstream analysis of 16S taxonomic data, and plots were made with the ggplot2 package (93).

Deposition of data. 16S rDNA sequencing data is deposited with the SRA under accession no. PRJNA445968 (https://www.ncbi.nlm.nih.gov/bioproject/PRJNA445968). Code used for 16S analysis is available at https://wipperman.github.io/TBRU/.

Statistics. Raw OTU count data was normalized using DESeq2 (94), and OTU abundances were individually correlated using Spearman correlation coefficients against the immunophenotypes described herein. Significant OTUs ($P < 0.01$) were plotted as a function of immune phenotype. To test whether there were differences between groups, we employed PERMANOVA using the adonis function in the Vegan R package, which partitions a distance matrix of OTU count data and runs 1-way ANOVA between groups of samples. To investigate microbiomic differences between family contacts of active pulmonary TB patients and healthy community controls, we ran LEfSe on DESeq normalized OTU count data (57). This technique employs nonparametric Kruskal-Wallis (KW) sum-rank test between each group ($P < 0.01$), followed by LDA to estimate the size of the effect. OTUs that were both differentially abundant between contacts and controls and that correlated with a particular immune phenotype were considered candidates for further analysis. All flow cytometry data analysis was performed using FCS Express (De Novo Software) and Prism 7 (GraphPad Software). Differences between cohorts were analyzed for statistical significance using unpaired or paired 2-tailed parametric *t* tests; $*P < 0.05$, $**P < 0.05$, $***P < 0.005$, and $****P < 0.0001$.

Study approval. All volunteers provided written informed consent to participate in this study. All human studies were reviewed and approved by the IRBs of both WCM and GHESKIO. Donors provided informed consent prior to peripheral blood draw for mononuclear cell isolation and stool collection for DNA extraction and 16S rDNA sequencing. All methods and procedures were performed in accordance with the relevant institutional guidelines and regulations.

Author contributions

Patient recruitment, enrollment, and sample collection were contributed by MAJ and DF; experiments were performed by CKV and MFW; assay development and analysis was contributed by CKV, MFW, KL, JB, MA, SB, VB, PW, JA, and MG; reagents were provided by KL and JA; and the paper was written by CKV, MFW, and MG.

Acknowledgments

We thank Rui Gardner, Paul Byrne, Christi O'Donnell, Mark Kweens, Erika Ritter, Sean Burke, Ashutosh Chaudhry, Sasha Rudensky, Olivier Levy, the Ludwig Center for Cancer Immunotherapy, and the MSKCC Immune Monitoring, Flow Cytometry, and Molecular Microbiology Core Facilities for their expert consultation. This study was supported by The Tri-I TRBU, part of the TBRU Network (U19 AI111143), and P30 CA008748. MFW acknowledges support from the National Center for Advancing Translational Sciences (grant TL1TR002386-01). CKV acknowledges support from the NIAID T32 Pathogenesis of Infectious Diseases Training Program (T32AI007613-18; Roy Gulick, WCM), the IDSA Education and Research Foundation Postdoctoral Fellowship Award in Infectious Diseases, and NIAID K08AI132739-01A1 (to CKV).

Address correspondence to: Michael S. Glickman, 417 E 68th Street, Z15, New York, New York 10065, USA. Phone: 646.888.2368; Email: glickmam@mskcc.org.

1. [No authors listed]. Global Tuberculosis Report. World Health Organization. http://www.who.int/tb/publications/global_report/en/. Accessed September 11, 2018.
2. Sizemore CF, Schleif AC, Bernstein JB, Heilman CA. The role of biomedical research in global tuberculosis control: gaps and challenges: A perspective from the US National Institute of Allergy and Infectious Diseases, National Institutes of Health. *Emerg Microbes Infect*. 2012;1(7):e9.
3. Jayashankar L, Hafner R. Adjunct Strategies for Tuberculosis Vaccines: Modulating Key Immune Cell Regulatory Mechanisms to Potentiate Vaccination. *Front Immunol*. 2016;7:577.
4. Bhatt K, Verma S, Ellner JJ, Salgame P. Quest for correlates of protection against tuberculosis. *Clin Vaccine Immunol*. 2015;22(3):258–266.
5. Bloom CI, et al. Transcriptional blood signatures distinguish pulmonary tuberculosis, pulmonary sarcoidosis, pneumonias and lung cancers. *PLoS One*. 2013;8(8):e70630.
6. Berry MP, et al. An interferon-inducible neutrophil-driven blood transcriptional signature in human tuberculosis. *Nature*. 2010;466(7309):973–977.
7. Braun MM, et al. Increasing incidence of tuberculosis in a prison inmate population. Association with HIV infection. *JAMA*. 1989;261(3):393–397.
8. Diedrich CR, et al. Reactivation of latent tuberculosis in cynomolgus macaques infected with SIV is associated with early peripheral T cell depletion and not virus load. *PLoS One*. 2010;5(3):e9611.
9. Gallegos AM, van Heijst JW, Samstein M, Su X, Pamer EG, Glickman MS. A gamma interferon independent mechanism of CD4 T cell mediated control of M. tuberculosis infection in vivo. *PLoS Pathog*. 2011;7(5):e1002052.
10. Sakai S, et al. CD4 T Cell-Derived IFN-γ Plays a Minimal Role in Control of Pulmonary Mycobacterium tuberculosis Infection and Must Be Actively Repressed by PD-1 to Prevent Lethal Disease. *PLoS Pathog*. 2016;12(5):e1005667.
11. Marakalala MJ, et al. Inflammatory signaling in human tuberculosis granulomas is spatially organized. *Nat Med*. 2016;22(5):531–538.
12. Nunes-Alves C, et al. Human and Murine Clonal CD8+ T Cell Expansions Arise during Tuberculosis Because of TCR Selection. *PLoS Pathog*. 2015;11(5):e1004849.
13. Godfrey DI, Uldrich AP, McCluskey J, Rossjohn J, Moody DB. The burgeoning family of unconventional T cells. *Nat Immunol*. 2015;16(11):1114–1123.
14. Zajonc DM, Flajnik MF. CD1, MR1, NKT, and MAIT: evolution and origins of non-peptidic antigen recognition by T lymphocytes. *Immunogenetics*. 2016;68(8):489–490.
15. Fischer K, et al. Mycobacterial phosphatidylinositol mannoside is a natural antigen for CD1d-restricted T cells. *Proc Natl Acad Sci USA*. 2004;101(29):10685–10690.
16. Rothchild AC, Jayaraman P, Nunes-Alves C, Behar SM. iNKT cell production of GM-CSF controls Mycobacterium tuberculosis. *PLoS Pathog*. 2014;10(1):e1003805.
17. Chancellor A, et al. Quantitative and qualitative iNKT repertoire associations with disease susceptibility and outcome in macaque tuberculosis infection. *Tuberculosis (Edinb)*. 2017;105:86–95.
18. Sutherland JS, et al. High granulocyte/lymphocyte ratio and paucity of NKT cells defines TB disease in a TB-endemic setting. *Tuberculosis (Edinb)*. 2009;89(6):398–404.
19. Montoya CJ, et al. Characterization of human invariant natural killer T subsets in health and disease using a novel invariant natural killer T cell-clonotypic monoclonal antibody, 6B11. *Immunology*. 2007;122(1):1–14.
20. Im JS, et al. Alteration of the relative levels of iNKT cell subsets is associated with chronic mycobacterial infections. *Clin Immunol*. 2008;127(2):214–224.
21. Dusseaux M, et al. Human MAIT cells are xenobiotic-resistant, tissue-targeted, CD161hi IL-17-secreting T cells. *Blood*. 2011;117(4):1250–1259.
22. Treiner E, et al. Selection of evolutionarily conserved mucosal-associated invariant T cells by MR1. *Nature*. 2003;422(6928):164–169.
23. Le Bourhis L, et al. MAIT cells detect and efficiently lyse bacterially-infected epithelial cells. *PLoS Pathog*. 2013;9(10):e1003681.
24. Eckle SB, et al. Recognition of Vitamin B Precursors and Byproducts by Mucosal Associated Invariant T Cells. *J Biol Chem*. 2015;290(51):30204–30211.
25. Reantragoon R, et al. Antigen-loaded MR1 tetramers define T cell receptor heterogeneity in mucosal-associated invariant T

cells. *J Exp Med*. 2013;210(11):2305–2320.
26. Rahimpour A, et al. Identification of phenotypically and functionally heterogeneous mouse mucosal-associated invariant T cells using MR1 tetramers. *J Exp Med*. 2015;212(7):1095–1108.
27. Treiner E, et al. Selection of evolutionarily conserved mucosal-associated invariant T cells by MR1. *Nature*. 2003;422(6928):164–169.
28. Le Bourhis L, et al. Antimicrobial activity of mucosal-associated invariant T cells. *Nat Immunol*. 2010;11(8):701–708.
29. Zabijak L, et al. Increased tumor infiltration by mucosal-associated invariant T cells correlates with poor survival in colorectal cancer patients. *Cancer Immunol Immunother*. 2015;64(12):1601–1608.
30. Pellicci DG, et al. Differential recognition of CD1d-alpha-galactosyl ceramide by the V beta 8.2 and V beta 7 semi-invariant NKT T cell receptors. *Immunity*. 2009;31(1):47–59.
31. Chiba A, et al. Activation status of mucosal-associated invariant T cells reflects disease activity and pathology of systemic lupus erythematosus. *Arthritis Res Ther*. 2017;19(1):58.
32. Hayashi E, et al. Involvement of Mucosal-associated Invariant T cells in Ankylosing Spondylitis. *J Rheumatol*. 2016;43(9):1695–1703.
33. Leeansyah E, Loh L, Nixon DF, Sandberg JK. Acquisition of innate-like microbial reactivity in mucosal tissues during human fetal MAIT-cell development. *Nat Commun*. 2014;5:3143.
34. Gold MC, et al. Human mucosal associated invariant T cells detect bacterially infected cells. *PLoS Biol*. 2010;8(6):e1000407.
35. Li K, et al. Synthesis, stabilization, and characterization of the MR1 ligand precursor 5-amino-6-D-ribitylaminouracil (5-A-RU). *PLoS ONE*. 2018;13(2):e0191837.
36. Kurioka A, et al. MAIT cells are licensed through granzyme exchange to kill bacterially sensitized targets. *Mucosal Immunol*. 2015;8(2):429–440.
37. Jiang J, et al. Mucosal-associated invariant T-cell function is modulated by programmed death-1 signaling in patients with active tuberculosis. *Am J Respir Crit Care Med*. 2014;190(3):329–339.
38. Jiang J, et al. Mucosal-associated invariant T cells from patients with tuberculosis exhibit impaired immune response. *J Infect*. 2016;72(3):338–352.
39. Kwon YS, et al. Mucosal-associated invariant T cells are numerically and functionally deficient in patients with mycobacterial infection and reflect disease activity. *Tuberculosis (Edinb)*. 2015;95(3):267–274.
40. Coulter F, et al. IL-17 Production from T Helper 17, Mucosal-Associated Invariant T, and γδ Cells in Tuberculosis Infection and Disease. *Front Immunol*. 2017;8:1252.
41. Seshadri C, et al. A polymorphism in human MR1 is associated with mRNA expression and susceptibility to tuberculosis. *Genes Immun*. 2017;18(1):8–14.
42. Paquin-Proulx D, et al. Latent Mycobacterium tuberculosis Infection Is Associated With a Higher Frequency of Mucosal-Associated Invariant T and Invariant Natural Killer T Cells. *Front Immunol*. 2018;9:1394.
43. Shen Y, et al. Adaptive immune response of Vgamma2Vdelta2+ T cells during mycobacterial infections. *Science*. 2002;295(5563):2255–2258.
44. Huang D, et al. Clonal immune responses of Mycobacterium-specific γδ T cells in tuberculous and non-tuberculous tissues during M. tuberculosis infection. *PLoS ONE*. 2012;7(2):e30631.
45. Pinheiro MB, et al. CD4-CD8-αβ and γδ T cells display inflammatory and regulatory potentials during human tuberculosis. *PLoS One*. 2012;7(12):e50923.
46. Chen CY, et al. Phosphoantigen/IL2 expansion and differentiation of Vγ2Vδ2 T cells increase resistance to tuberculosis in non-human primates. *PLoS Pathog*. 2013;9(8):e1003501.
47. del Corral H, et al. IFNgamma response to Mycobacterium tuberculosis, risk of infection and disease in household contacts of tuberculosis patients in Colombia. *PLoS One*. 2009;4(12):e8257.
48. Ueta C, Tsuyuguchi I, Kawasumi H, Takashima T, Toba H, Kishimoto S. Increase of gamma/delta T cells in hospital workers who are in close contact with tuberculosis patients. *Infect Immun*. 1994;62(12):5434–5441.
49. Corbett AJ, et al. T-cell activation by transitory neo-antigens derived from distinct microbial pathways. *Nature*. 2014;509(7500):361–365.
50. Eckle SB, et al. A molecular basis underpinning the T cell receptor heterogeneity of mucosal-associated invariant T cells. *J Exp Med*. 2014;211(8):1585–1600.
51. Kurioka A, et al. Shared and Distinct Phenotypes and Functions of Human CD161++ Vα7.2+ T Cell Subsets. *Front Immunol*. 2017;8:1031.
52. Gherardin NA, et al. Human blood MAIT cell subsets defined using MR1 tetramers. *Immunol Cell Biol*. 2018;96(5):507–525.
53. Gallegos AM, et al. Control of T cell antigen reactivity via programmed TCR downregulation. *Nat Immunol*. 2016;17(4):379–386.
54. Arpaia N, et al. Metabolites produced by commensal bacteria promote peripheral regulatory T-cell generation. *Nature*. 2013;504(7480):451–455.
55. Schirmer M, et al. Linking the Human Gut Microbiome to Inflammatory Cytokine Production Capacity. *Cell*. 2016;167(4):1125–1136.e8.
56. Omenetti S, Pizarro TT. The Treg/Th17 Axis: A Dynamic Balance Regulated by the Gut Microbiome. *Front Immunol*. 2015;6:639.
57. Segata N, et al. Metagenomic biomarker discovery and explanation. *Genome Biol*. 2011;12(6):R60.
58. Janis EM, Kaufmann SH, Schwartz RH, Pardoll DM. Activation of gamma delta T cells in the primary immune response to Mycobacterium tuberculosis. *Science*. 1989;244(4905):713–716.
59. Adams EJ, Gu S, Luoma AM. Human gamma delta T cells: Evolution and ligand recognition. *Cell Immunol*. 2015;296(1):31–40.
60. Tanaka Y, et al. Nonpeptide ligands for human gamma delta T cells. *Proc Natl Acad Sci USA*. 1994;91(17):8175–8179.
61. Nerdal PT, et al. Butyrophilin 3A/CD277-Dependent Activation of Human γδ T Cells: Accessory Cell Capacity of Distinct Leukocyte Populations. *J Immunol*. 2016;197(8):3059–3068.
62. Gu S, Nawrocka W, Adams EJ. Sensing of Pyrophosphate Metabolites by Vγ9Vδ2 T Cells. *Front Immunol*. 2014;5:688.
63. Spencer CT, Abate G, Blazevic A, Hoft DF. Only a subset of phosphoantigen-responsive gamma9delta2 T cells mediate protec-

tive tuberculosis immunity. *J Immunol*. 2008;181(7):4471–4484.
64. Tsukaguchi K, Balaji KN, Boom WH. CD4+ alpha beta T cell and gamma delta T cell responses to Mycobacterium tuberculosis. Similarities and differences in Ag recognition, cytotoxic effector function, and cytokine production. *J Immunol*. 1995;154(4):1786–1796.
65. Qaqish A, et al. Adoptive Transfer of Phosphoantigen-Specific γδ T Cell Subset Attenuates Mycobacterium tuberculosis Infection in Nonhuman Primates. *J Immunol*. 2017;198(12):4753–4763.
66. Dieli F, et al. Ligand-specific alphabeta and gammadelta T cell responses in childhood tuberculosis. *J Infect Dis*. 2000;181(1):294–301.
67. Sutton CE, Mielke LA, Mills KH. IL-17-producing γδ T cells and innate lymphoid cells. *Eur J Immunol*. 2012;42(9):2221–2231.
68. Li B, et al. Disease-specific changes in gammadelta T cell repertoire and function in patients with pulmonary tuberculosis. *J Immunol*. 1996;157(9):4222–4229.
69. Hong BY, Maulén NP, Adami AJ, Granados H, Balcells ME, Cervantes J. Microbiome Changes during Tuberculosis and Anti-tuberculous Therapy. *Clin Microbiol Rev*. 2016;29(4):915–926.
70. Wipperman MF, et al. Antibiotic treatment for Tuberculosis induces a profound dysbiosis of the microbiome that persists long after therapy is completed. *Sci Rep*. 2017;7(1):10767.
71. Maji A, et al. Gut microbiome contributes to impairment of immunity in pulmonary tuberculosis patients by alteration of butyrate and propionate producers. *Environ Microbiol*. 2018;20(1):402–419.
72. Namasivayam S, et al. Longitudinal profiling reveals a persistent intestinal dysbiosis triggered by conventional anti-tuberculosis therapy. *Microbiome*. 2017;5(1):71.
73. Glynn JR, Murray J, Bester A, Nelson G, Shearer S, Sonnenberg P. High rates of recurrence in HIV-infected and HIV-uninfected patients with tuberculosis. *J Infect Dis*. 2010;201(5):704–711.
74. Verver S, et al. Rate of reinfection tuberculosis after successful treatment is higher than rate of new tuberculosis. *Am J Respir Crit Care Med*. 2005;171(12):1430–1435.
75. Mosites E, et al. Microbiome sharing between children, livestock and household surfaces in western Kenya. *PLoS One*. 2017;12(2):e0171017.
76. Song SJ, et al. Cohabiting family members share microbiota with one another and with their dogs. *Elife*. 2013;2:e00458.
77. Wexler HM. Bacteroides: the good, the bad, and the nitty-gritty. *Clin Microbiol Rev*. 2007;20(4):593–621.
78. Dasgupta S, Erturk-Hasdemir D, Ochoa-Reparaz J, Reinecker HC, Kasper DL. Plasmacytoid dendritic cells mediate anti-inflammatory responses to a gut commensal molecule via both innate and adaptive mechanisms. *Cell Host Microbe*. 2014;15(4):413–423.
79. Koay HF, et al. A three-stage intrathymic development pathway for the mucosal-associated invariant T cell lineage. *Nat Immunol*. 2016;17(11):1300–1311.
80. Meermeier EW, et al. Human TRAV1-2-negative MR1-restricted T cells detect S. pyogenes and alternatives to MAIT riboflavin-based antigens. *Nat Commun*. 2016;7:12506.
81. Chen Z, et al. Mucosal-associated invariant T-cell activation and accumulation after in vivo infection depends on microbial riboflavin synthesis and co-stimulatory signals. *Mucosal Immunol*. 2017;10(1):58–68.
82. Ussher JE, et al. TLR signaling in human antigen-presenting cells regulates MR1-dependent activation of MAIT cells. *Eur J Immunol*. 2016;46(7):1600–1614.
83. Dias J, Leeansyah E, Sandberg JK. Multiple layers of heterogeneity and subset diversity in human MAIT cell responses to distinct microorganisms and to innate cytokines. *Proc Natl Acad Sci USA*. 2017;114(27):E5434–E5443.
84. Constantinides MG. Interactions between the microbiota and innate and innate-like lymphocytes. *J Leukoc Biol*. 2018;103(3):409–419.
85. Nielsen MM, Witherden DA, Havran WL. γδ T cells in homeostasis and host defence of epithelial barrier tissues. *Nat Rev Immunol*. 2017;17(12):733–745.
86. Paquin-Proulx D, et al. Bacteroides are associated with GALT iNKT cell function and reduction of microbial translocation in HIV-1 infection. *Mucosal Immunol*. 2017;10(1):69–78.
87. Edgar RC. UPARSE: highly accurate OTU sequences from microbial amplicon reads. *Nat Methods*. 2013;10(10):996–998.
88. Camacho C, et al. BLAST+: architecture and applications. *BMC Bioinformatics*. 2009;10:421.
89. NCBI Resource Coordinators . Database resources of the National Center for Biotechnology Information. *Nucleic Acids Res*. 2018;46(D1):D8–D13.
90. McDonald D, et al. The Biological Observation Matrix (BIOM) format or: how I learned to stop worrying and love the omeome. *Gigascience*. 2012;1(1):7.
91. R Core Team. R: A language and environment for statistical computing. R Foundation for Statistical Computing, Vienna, Austria. http://www.R-project.org/. Accessed September 11, 2018.
92. McMurdie PJ, Holmes S. phyloseq: an R package for reproducible interactive analysis and graphics of microbiome census data. *PLoS One*. 2013;8(4):e61217.
93. Wickham H. *Ggplot2: elegant graphics for data analysis*. New York, New York: Springer; 2009.
94. Love MI, Huber W, Anders S. Moderated estimation of fold change and dispersion for RNA-seq data with DESeq2. *Genome Biol*. 2014;15(12):550.